*Invited Paper*

# Applications of Ultrafast Lasers in Microfabrication

Michael M. MIELKE, Timothy BOOTH, Michael GREENBERG, David M. GAUDIOSI, Carolyn MARTINEZ, Steven P. SAPERS, Robert CLINE and Ramanujapuram A. SRINIVAS

*Raydiance, Inc., 1450 North McDowell Blvd., Petaluma, CA 94954*
*E-mail: mmielke@raydiance.com*

Just as photolithography technology brought about the miniaturization of integrated circuits and drove multiple market opportunities in the electronics sector, a similar inflection point has arrived for ultrafast lasers. While these femtosecond class lasers have long enabled the precise manipulation of matter without heat affects, only recently, with the advent of commercial grade systems, has the potential of the technology been realized. Fiber optic architecture, embedded software control and robust telecom components have been leveraged to ensure the reliability, ease of use, and performance standards required in manufacturing settings. With femtosecond laser microfabrication tools now accessible to industry, the relevance of femtosecond lasers to modern manufacturing has become clear based on compelling economics, unparalleled precision, and new flexibility with respect to materials. These new capabilities are opening up enormous opportunities in automotive components, consumer electronics, medical devices, aerospace and bioscience applications.
DOI:10.2961/jlmn.2013.02.0001

**Keywords:** Ultrafast lasers, femtosecond lasers, materials processing, athermal machining, advanced manufacturing, precision microfabrication

## 1. Introduction

When delivered properly to the target, the high peak power and extreme brevity of femtosecond laser pulses enable material removal through photo-ionization without imposing thermal effects on the remaining structure [1]. This predominantly athermal ablation phenomenon is beyond the reach of ultraviolet excimer lasers and nanosecond pulse lasers which necessarily deposit substantial heat in the substrate resulting in heat affected zones (HAZ) [2]. Instead, the modification provided by femtosecond lasers supports precision fabrication of devices that cannot be achieved by any other practical technique.

Fabrication process impact includes dramatic reduction of post-processing requirements for metal devices since deleterious side effects, such as recast, dross, and HAZ, can be substantially reduced. Moreover, precision modification and machining of difficult-to-process materials, such as polymers and brittle dielectrics, are enabled by femtosecond laser methods. Key benefits include laser precision machining of new classes of materials, higher device manufacturing throughput speed and yield in many industrial processes, and significantly reduced complexity and direct labor versus incumbent device fabrication techniques.

Over the past several years, Raydiance has pioneered the ultrafast laser microfabrication industry by first proving that commercial grade femtosecond lasers are practical, then by validating the need for these systems in high value manufacturing lines. In this paper, we will describe the three key aspects that have validated femtosecond laser commercial microfabrication: compelling economics, unparalleled precision, and new materials flexibility. For completeness, we start with a brief summary of femtosecond laser machining along with an overview of commercial grade femtosecond laser sources. These background topics are followed by a review of the validation factors applied to manufacturing of modern fuel injectors for internal combustion engines.

## 2. Femtosecond Laser Machining

There has been considerable dialogue in the laser materials processing community regarding the enabling pulse duration for achieving athermal ablation—where the remaining material shows negligible HAZ [2]. The specific solution is process dependent since the laser repetition rate as well as the material feed rate influence spatial heat build-up. It should be noted that even a femtosecond pulse train, if applied too quickly to a confined target area, can produce appreciable thermal effects. Nonetheless, there are general trends that have been well documented, including a pulse width requirement based upon the physical properties of a given material.

The pulse width regime for nonthermal ablation is defined by $\tau_p << (\delta^2/D)$, where $\tau_p$ is the laser pulse duration full width at half maximum (FWHM) power, $\delta$ is the optical skin depth, and $D$ is the thermal diffusivity of the material [3]. There is some variety in the pulse width requirements for different materials since the electron-phonon coupling time can range from less than one picosecond to several tens of picoseconds [4]. Moreover, this condition holds for single pulse fluence near the ablation threshold. Well above threshold, there is generally a downward trend—to shorter pulse duration—required for athermal ablation [5].

In addition to defining the inflection point where the process transitions to being athermal, the laser pulse duration plays a large role in the material removal rate since pulse energy that contributes to thermally damaging the target substrate is not efficiently contributing to material removal. As example, we illustrate a significant change in slope for Nitinol machining rate versus pulse duration that occurs near 1.2 ps. Complete details of this experiment are

provided in [6] and are summarized here to help the reader understand the importance of laser selection and pulse width stability for machining efficacy.

In order to maximize relevance to real applications, we chose Nitinol, a nickel-titanium shape memory alloy, as the material for analysis since it is widely used for the manufacture of cardiovascular stents and other medical devices—a primary commercial application for ultrafast lasers. The raw tubing has typical dimensions for stents: 1.83 mm (0.072") outer diameter and 267 μm wall thickness. The tubing is positioned in a standard stent cutting workstation comprising a laser lathe style motion control system (Rofin StarCut Tube), a Raydiance R-100 laser system, and beam delivery head capable of coaxial gas flow to the target. Machining time is measured by recording the signal from a visible light photodiode that is positioned adjacent to the ablation site. Strong visible spectrum light is emitted by the ablation plasma, and with the use of a high speed oscilloscope, the rising and trailing edges of this emission provide accurate temporal markers for the start and stop of machining [7].

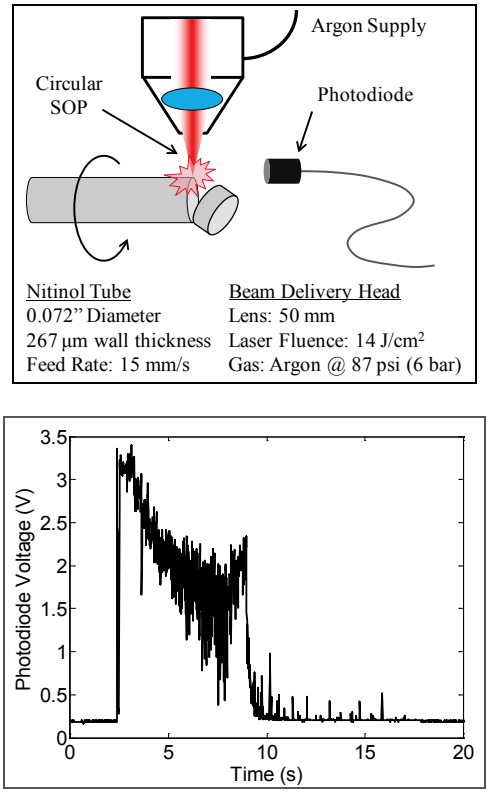


**Fig. 1**: Experimental set-up for the Nitinol machining rate tests (top) and an example machining interval measurement using the visible light photodiode to monitor plasma emission (bottom). SOP – state of polarization.

Fig. 1 top and bottom show, respectively, a functional sketch of the Nitinol machining rate measurement set-up and an example measurement of the machining time to cut a washer. We cut washers, or little rings of material, from the end of a Nitinol tube using continuous tube rotation with a linear feed rate of 15 mm/s (0.6 in/s) in the plane of beam focus, and we measured the total time to cut each washer at the different pulse durations. We selected this simple machining routine for the comparison since it removes pattern dependence and incubation effects [8] that can skew observations of fundamental ablation rate.

The laser parameters are: 1552 nm wavelength, 44 μJ pulse energy, 100 kHz pulse repetition rate (4.4 W average power), 6 mm beam diameter entering the focusing lens, beam quality $M^2 < 1.2$, and tunable pulse duration from 677 fs to 12.7 ps. Pulse duration is tuned by modifying the inter-grating distance by <5 mm in our Treacy pulse compressor. Pulse energy, and all other laser parameters, is held constant as pulse width is tuned. Beam quality was verified to be consistent over this small (<1% inter-grating distance change) tuning range. The beam is focused using a 50 mm focal length Gradium lens (Lightpath) to approximately 20 μm spot diameter at the tube surface for a fluence of 14 J/cm$^2$. The beam exits the delivery head (Laser Mechanisms) through a nozzle to provide on-axis purge gas (6 bar argon). The nozzle stand-off from the tube is 254 μm (0.010").

Eleven washers were cut at each pulse duration from 677 fs to 12.7 ps in order to gather a modest statistical distribution. The mean washer cut-off times and the net fluence deposited in the part (cut-off time × laser power) are shown in Fig. 2. The independent error bars for each data marker correspond to the standard deviation for each set. The chart also shows linear trend lines leading away from the inflection point near 1.2 ps. Above this point, the slope of cut-off time versus pulse duration is four times higher than below this point, indicating a strong shift in the fundamental ablation phenomenon. Moreover, it should be noted that the washer cut-off time for 12.7 ps pulse duration is 2.5 times longer than at 677 fs. This is likely the result of increasing proportion of pulse energy deposited as heat for these longer pulse durations.

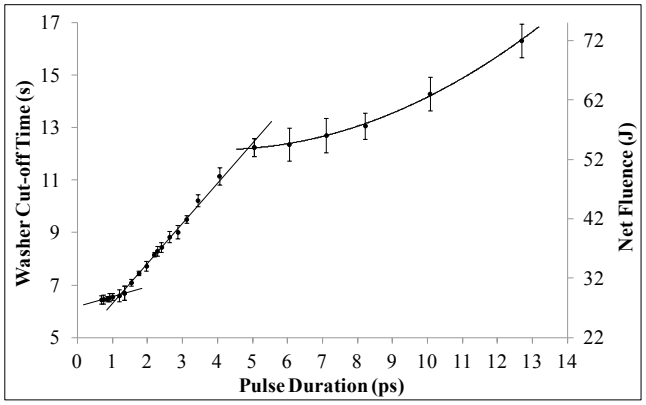


**Fig. 2**: Nitinol washer cut-off time (left axis) and net fluence applied (right axis) vs. laser pulse duration in the ultrafast regime [6].

The notable kink in the longer pulse dependency that occurs near 5 ps is possibly the result of a phonon resonance that impacts material removal rate, since the electron-phonon relaxation times for the constituent metals are relatively close to this value, e.g. nickel has relaxation time of 7 ps [9]. It should also be noted that the standard deviation values (error bars) increase with increasing pulse duration. This is likely a result of the stochastic nature of ionization-induced laser ablation, and tighter confinement of

pulse energy with shorter pulses yields a more deterministic event [10].

The simple experiment comparing machining speed (washer cut-off time) versus pulse duration reveals the critical difference in laser machining efficacy using femtosecond-class lasers. This illustrates both the benefit of processing materials in the femtosecond regime as well as the need for highly stable and reliable femtosecond laser sources to service the microfabrication industry. In the next section, we describe what it means to be a commercial grade femtosecond system and how the Raydiance platform sets the standard for performance.

## 3. Commercial Grade Systems

Femtosecond lasers have existed in research laboratories for more than three decades. In the late 1980's, there was a renaissance of femtosecond research applications with the advent of the titanium sapphire solid-state laser [11]. Still, femtosecond laser applications remained stuck in the academic laboratory until only very recently, with the emergence of higher energy and power, fiber-optic and thin disk femtosecond laser architectures [12][13]. Raydiance's laser systems feature a fiber-optic architecture using erbium amplifiers and telecommunications C-band components. This architecture was chosen for benefit from the global investment in optical telecommunications infrastructure for the past two decades, and to leverage the robust, mature supply chain for C-band components and systems [14]. Moreover, single mode, monolithic fiber-optic systems benefit from intrinsic stability and excellent beam quality owing to the guided wave beam path [15].

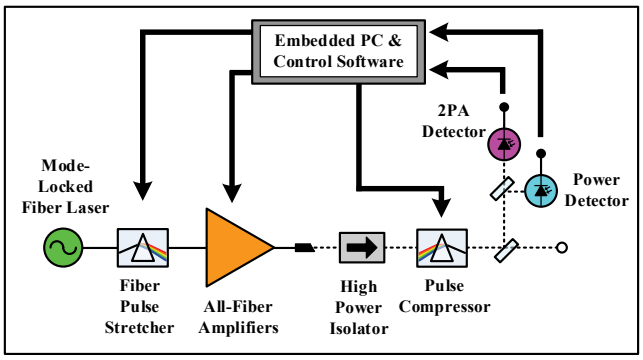


**Fig. 3:** High-level schematic of the Raydiance fiber-optic femtosecond laser architecture with computer controlled, closed-loop stabilization of critical laser parameters such as power and pulse duration. PC: personal computer. 2PA: two-photon absorption.

Fig. 3 shows a high-level schematic of the primarily fiber-optic laser architecture with closed loop software control of laser power and femtosecond class pulse duration. Ultra-short optical pulses are initially generated with low energy in a mode-locked fiber laser then amplified to the 50 μJ level using the well-known chirped pulse amplification (CPA) technique [16]. In the R-100 laser system, the pulse stretcher comprises a pair of chirped fiber Bragg gratings (CFBG) and a four-port fiber circulator. Three erbium fiber amplifier stages provide the required net optical gain for the system (~60 dB), and a fiber-pigtailed acousto-optic modulator (AOM) reduces the pulse repetition rate from 40 MHz to 100 kHz (or another sub-harmonic) between the first and second amplifiers. Pulses are compressed in a free-space, dual diffraction grating compressor, and the amplifiers are protected from any subsequent back-reflections using a high power, double-stage optical isolator. The output signal is sampled by both an InGaAs photodiode power monitor and a silicon photodiode used in two-photon absorption (2PA) mode. The latter provides a relative measurement of pulse duration since shorter pulses will produce stronger 2PA signal [17]. Finally, electrical signals from these sensors are monitored by an internal Linux based operating system residing in a single-board computer inside the laser housing. This software control system adjusts system dispersion (stretcher and compressor) as well as amplifier pump current in order to maintain constant output power and pulse duration.

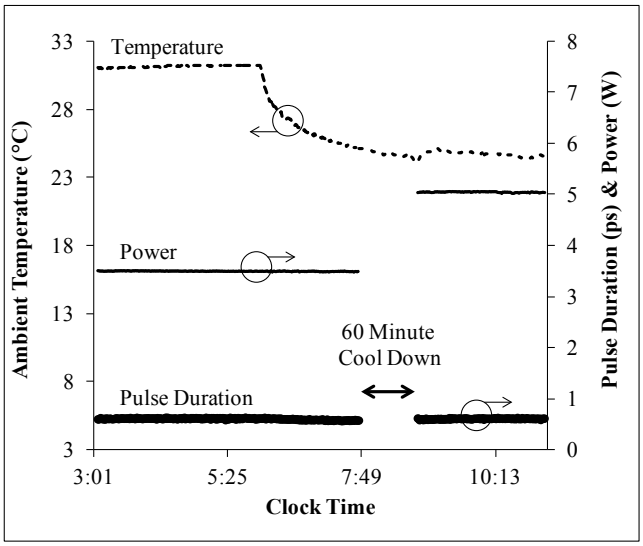


**Fig. 4:** Average laser power (thin, solid line) and pulse width (thick, solid line) vs. clock time. Ambient temperature (dash line) is allowed to drift as part of stability testing.

Fig. 4 shows a typical long term operating measurement for an R-100 laser unit during its factory burn-in test. Over an 8-hour period, the room temperature changes by 7 °C, and the laser power set-point is shifted from 3.5 W to 5 W by user command. The power shift by command includes a complete cool down (60 minutes) to intentionally stress the control system. Nonetheless, the laser pulse duration is highly stable over the whole operating period. Fig. 5 shows pulse duration vs. clock time (same data as Fig. 4) with a narrow vertical scale range. The pulse duration mean is 701 fs and the variation is 4%. This variation measurement is actually measurement instrument limited, since intensity autocorrelators are not yet available in commercial grade form factor. All measurements follow ISO protocol for laser stability testing [18].

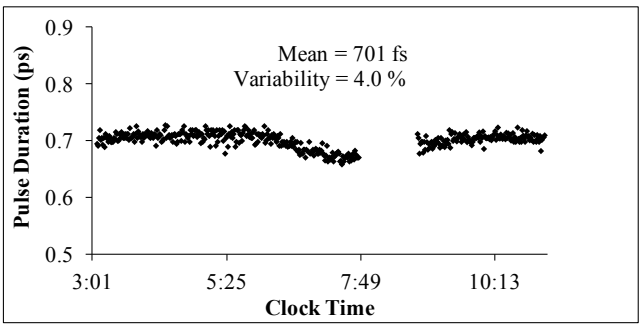


**Fig. 5:** Closer detail of pulse duration vs. clock time.

The novel advances that provide this level of laser stability are autonomously-controlled laser average power and pulse quality using embedded sensors and tuning elements. Average power is detected after each fiber amplifier stage by standard telecom optical performance monitors (OPM) comprising ~1% power taps and InGaAs photodiodes. Average power is adjusted by controlling fiber amplifier pump diode current and/or by controlling radio frequency (RF) power injected into an output stage acousto-optic modulator (AOM). Pulse quality is detected using the 2PA photodiode after the pulse compressor [17], and pulse quality is adjusted by controlling the inter-grating distance in the pulse compressor using a motorized linear translation stage.

Further details of the laser stability performance and control system mechanisms are provided in [19]. The salient point here is that the advanced microfabrication capabilities of femtosecond lasers are only accessible to industrial manufacturing when the complexity of sustaining the optimally compressed pulse, along with maintaining all other system parameters, is managed by an internal, closed-loop software operating system. Moreover, owing to its well-integrated optical, electrical and software subsystems, along with standard internet connectivity, the Raydiance laser system has unique capabilities for remote telemetry and service, which has proven very convenient for Raydiance users as these systems have been deployed into manufacturing facilities worldwide.

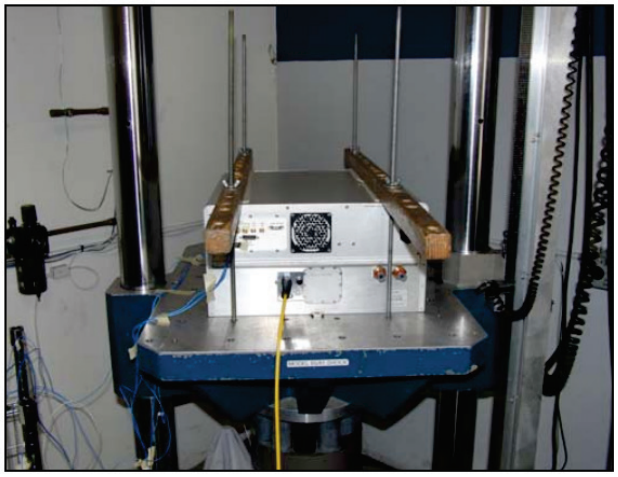

**Fig. 6:** Photograph of the Raydiance R-100 laser system output module mounted on the mechanical test table during standard shock resilience evaluation [20].

Another key attribute of commercial grade femtosecond lasers is robustness against misalignment, or other deleterious changes, during shipment and delivery of these systems into standard manufacturing work cells. To ensure unit-to-unit reliability, Raydiance products are evaluated for mechanical resilience to shock and vibration following standard ASTM protocol [20]. Fig. 6 shows a photograph of a Raydiance R-100 output module mounted on the top-to-bottom shock testing table during the execution of the suite of mechanical tests. System validation and test (SVT) procedures were executed before and after the shock and vibration testing—with no manual re-optimization of the laser—and confirmed that no discernable performance changes to the laser had occurred. Table 1 lists several of the key laser parameters that were measured and validated as unchanged before and after testing.

**Table 1:** Key parameters validated before and after shock and vibration testing of the R-100 laser system.

| Parameter | Spec. | Tolerance | Before | After |
|---|---|---|---|---|
| Pulse Duration | <700 fs | NA | Pass | Pass |
| Beam Quality | $M^2$<1.3 | NA | Pass | Pass |
| Power (W) | 5 | +5%, -0% | Pass | Pass |
| Beam Egress (mm) | 77.4 | <0.75 | Pass | Pass |

The numerous precision microfabrication applications that are uniquely provided by femtosecond lasers are now accessible to manufacturers of high value components owing to the development and deployment of commercial grade femtosecond lasers. In this section, we briefly described how Raydiance's laser system architecture—based on fiber optics and integrated software control system—provides the essential stability and reliability performance for consistent quality of precision in realistic manufacturing settings. In the following sections, we describe the dominant factors driving demand for femtosecond laser processing in todays industrial, consumer and medical device manufacturing markets.

## 4. Compelling Economics

Ultrafast laser material processing may not be the best solution for every single microfabrication challenge, since there must be a balance of three critical factors: quality of features, speed of processing, and overall expense of the process. Nonetheless, the breadth of microfabrication applications where ultrafast laser processing has the cost/benefit advantage is huge—both in terms of applications diversity and market volume.

Sixty four percent (64%) of the nine-billion-dollar ($9B) commercial laser market comprises lasers and workstations for materials processing [21]. Although ultrafast lasers represent only ~3% of the pulsed laser market for microfabrication, these lasers are recognized to have the fastest growing gain in market share [22]. Just as the early precision and speed advantages of continuous wave (CW) lasers, and subsequently nanosecond pulse lasers, drove demand for industrial deployment of these technologies, the increasing demands for greater precision at faster ma-

chining speeds is presently driving deployment of femtosecond laser workstations into high value manufacturing situations.

Femtosecond laser penetration into commercial manufacturing opportunities relies on two critical factors:

1. The quality of the fabricated feature cannot be achieved by any other *practical* means.
2. The cost benefit of switching to a femtosecond laser solution is readily apparent using a standard return-on-investment (ROI) calculation.

Commercial laser industry insiders typically consider the cost of laser products in isolation from other cost factors when discussing commercial laser options with consumers. This is not surprising, since this comparison favors incumbent technologies in their product portfolios. Nonetheless, such a comparison is misleading since it neglects critical factors such as the assortment of post-processing steps required to remove HAZ and other defects imposed by conventional lasers.

Comprehension of the full, end-to-end microfabrication process is even more important when comparing femtosecond laser solutions to non-laser techniques, such as mechanical machining and/or electrical discharge machining (EDM). For sake of brevity, we summarize the key differences between the incumbent microfabrication techniques and femtosecond laser solutions as:

- Mechanical: too slow, consumable tools, rough surface finish, and inflexible geometries.
- EDM: too slow, consumable electrodes, thermal damage, and inflexible geometries.
- CW, nanosecond, or picosecond laser: heat affected zone (HAZ) imposes chemical post-processing, also limits precision and flexibility.

While mechanical, EDM or alternative laser methods may impose lower capital equipment costs in many applications, none of these achieves the required feature quality at practical speeds in the most demanding microfabrication situations. To illustrate this point, we conducted a simple metal machining experiment to compare femtosecond laser processing to the nearest neighbor alternative, picosecond laser processing.

Fig. 7 shows a comparison of machined depth in stainless steel coupons using 700 fs pulses (top) vs. 10 ps pulses (bottom). These pulse durations represent groupings of commercial laser systems, i.e. 'femtosecond lasers' and 'picosecond lasers', respectively. Here we distinguish commercial purpose femtosecond lasers from scientific purpose femtosecond lasers since the latter often feature pulse duration of 100 fs or lower. The femtosecond and picosecond pulses machined depths of 72 μm and 30 μm, respectively. Consistency is ensured by using the exact same laser source and beam delivery conditions for both machining trials. The laser pulse duration shifts from 700 fs to 10 ps by adjusting the inter-grating distance in the laser pulse compressor. The 2x2 mm pockets were milled using a galvo scanner (ScanLab) with f-theta lens to maintain 82 μm spot diameter. 48 μJ pulses were delivered at 20 kHz repetition rate in a bidirectional raster fill pattern with a progressive scan orientation (alternating angle) to reduce pattern and incubation effects [8]. Nitrogen purge gas was directed at the coupons (off-axis, 25 psi at nozzle) to hasten debris removal.

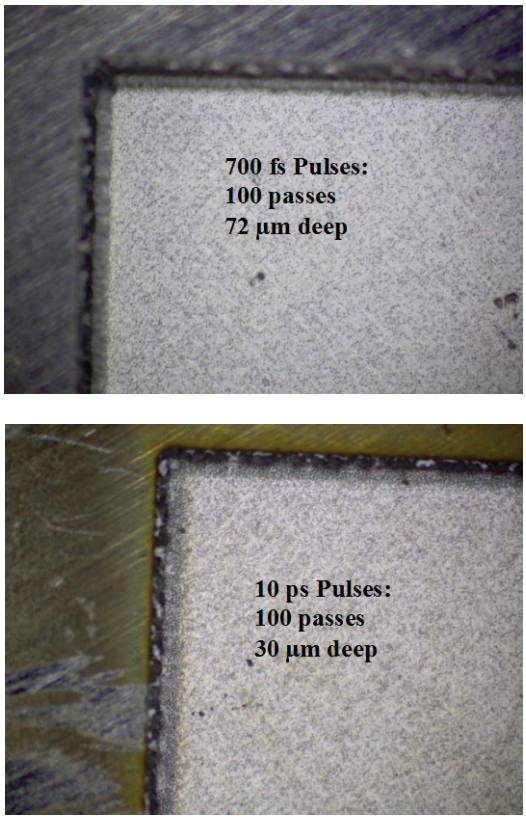


**Fig. 7:** Comparison of machined depth in stainless steel for 700 fs (top) vs. 10 ps (bottom) laser pulse duration. All other laser process parameters are held constant, including pulse energy, average power, wavelength, scanner pattern, ambient atmosphere and state of polarization.

It is clear from this side-by-side comparison that the 700 fs pulses remove material much more effectively than the 10 ps pulses when other process parameters are held constant. Moreover, the discoloration of the picosecond laser machined coupon (Color online) points to stronger heat diffusion into the area surrounding the ablation site. The disparate machining rate, and visible discoloration, point to the picosecond pulses having deposited more energy as heat in the substrate vs. the femtosecond pulses. The key here is that the 700 fs pulses have 14 times higher peak irradiance than the 10 ps pulses for equivalent pulse energy. Hence, the 700 fs pulses reach the ionization threshold much sooner during the rising edge of each pulse, electron-phonon energy transfer is diminished within the time frame of the pulse [3], and little energy is wasted through heat diffusion [4].

To further illustrate the criteria that motivates a manufacturer to upgrade to a femtosecond laser based material processing solution, we provide a brief, high level description of fabrication of fuel injector spray holes for gas direct injection (GDI) internal combustion engines.

In GDI engines, fuel is injected directly into the engine cylinder where combustion occurs. The advantages of this architecture are maintaining, or even increasing, the engine power output while using a lean-burn to reduce both fuel

consumption and $CO_2$ emissions [23]. Although there are multiple motivations for switching to GDI engines in cars and light trucks, a major reason the automobile industry is making the transition is U.S. government-mandated year-over-year improvement to fleet-wide automobile fuel efficiency [24]. GDI engine designers have identified precise control of the fuel spray pattern as a dominant factor in engine performance, and the spray pattern depends directly upon the geometry and surface quality of the machined spray nozzle holes [25].

Drilling the GDI spray nozzle holes with the required geometry and surface quality can, in principle, be achieved by several means. The key to femtosecond laser penetration of this market opportunity is that it is both practical to deploy in manufacturing and the cost-versus-benefit analysis for the femtosecond manufacturing solution shows a clear and compelling return on investment (ROI). The ROI criteria apply both to the capital equipment initial investment payback period (< 12 months) as well as the enhanced production line yield and elimination of consumable components from the machining process.

Salient success criteria for drilling GDI fuel injector spray holes include a ±1.5% tolerance on the hole area (±1.5 μm tolerance on 200 μm hole diameter) and an average surface roughness ($R_a$) < 200 nm. These figures of merit are due to the ±1.5% tolerance on fuel flow—which is directly proportional to hole area—along with the requirement for a consistent droplet spray pattern. Using a laser trepanning set-up with our femtosecond laser, we show deterministic drilling of GDI injector spray holes with ±1.4 μm tolerance on 200 μm hole diameter and $R_a$ < 100 nm. Moreover, we drill these holes with per hole cycle time < 2 s.

In contrast, the incumbent EDM drilling technique has standard tolerance of ±3.0 μm for holes in the diameter range of 100 to 400 μm. Hence, EDM-drilled holes are typically flow-tuned, using an abrasive fluid in a post-processing step, in order to reach the ±1.5% flow tolerance [26]. Furthermore, standard EDM drilling only achieves $R_a$ < 500 nm [27] and requires cycle time of 4 to 6 s for the GDI fuel injector hole size. Whereas the EDM-drilled hole diameter tolerance can be decreased (in theory) by using specialized electrodes, this option further increases the per hole cycle time. The EDM process also requires costly replacement of worn electrodes after a finite count of holes have been drilled.

For the reasons of drilled hole quality and speed of fabrication, the femtosecond laser solution provides a clear and compelling benefit to the economics of GDI fuel injector spray hole drilling. We have also analyzed the drilling process figures of merit when using a ~10 ps laser and found that the per hole cycle time increases to > 6 s in order to hold to similar hole quality. As noted above, this slower machining with a picosecond laser is the result of greater fractional heat deposit per pulse which lowers ablation efficiency and degrades drilled hole quality.

In this section we have illustrated the selection criteria that justify femtosecond laser solutions based on the clear economic benefit: superior fabricated feature quality while processing at speeds, or cycle times, that far surpass other practical methods. The next section will provide greater detail of the fuel injector spray nozzle hole drilling capability that we have achieved as well as illustrate the new spray nozzle geometry flexibility brought by femtosecond laser machining.

## 5. Greatest Precision

Fabrication precision is, of course, relative to the requirements of the industrial process being addressed. Whereas electron beam lithography systems can provide < 10 nm linewidths [28], the price of these systems (>$4M) makes them cost-prohibitive for most microfabrication situations. In a growing number of micro-manufacturing applications, commercial grade femtosecond lasers are providing the required precision and cost efficiency. In this section, we detail the precision micromachining capabilities of our femtosecond laser systems with respect to the fuel injector spray hole drilling application.

As noted in the previous section, precise control of the GDI fuel spray pattern is a dominant factor in engine performance, and the spray pattern depends directly upon the geometry and surface quality of the machined spray nozzle holes [25]. To maximize fuel economy and minimize emissions, the SAE gas fuel injector steering committee [29] recommends very tight control over:

- Flow
- Spray angle
- Drop size distribution
- Fuel mass distribution
- Spray tip penetration

Control of these parameters in high volume production of GDI fuel injectors is made deterministic and cost-effective by the hole-drilling performance revealed below.

Fig. 8 shows a scanning electron microscope (SEM) image (300x magnification) of a 200 μm diameter hole drilled through 250 μm thick stainless steel (316L) using a Raydiance R-200 laser and a multi-axis galvo scanner for laser trepanning. The 300x magnification SEM image reveals pristine substrate material (no heat affected zone), negligible taper of the hole (nominally 0°), and excellent surface roughness figure ($R_a$ < 0.1 μm). Laser process characteristics were: 45 μJ, 9 W (200 kHz) on target; helium purge gas (60 psi); and 1.3 s total drilling time.

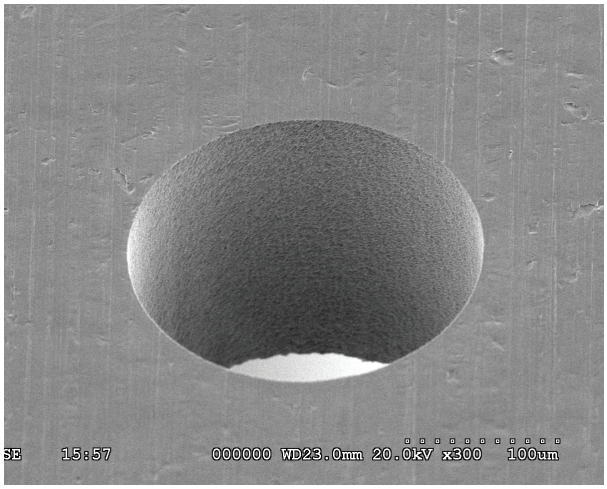


**Fig. 8:** Zero-taper, 200 μm diameter hole drilled in 250 μm thick stainless steel.

We analyzed the reproducibility and repeatability of this hole drilling process by measuring the diameters of the through-hole entrance and exit faces for 99 consecutive iterations of the process. The standard deviations for the entrance and exit face diameters are, respectively, 0.488 μm and 0.233 μm. The maximum variations for the entrance and exit face diameters are, respectively, 1.37 μm and 0.88 μm. We anticipate further optimization of the hole drilling algorithm can yield maximum diameter variation < 1 μm for similar hole geometry.

In addition to the basic zero-taper, circular hole drilling required currently for GDI fuel injector fabrication, the femtosecond laser trepanning solution enables new flexibility in terms of drilled hole geometry. Fig. 9 shows microscope images of an elliptical profile through-hole (top) and three side-by-side circular through-holes (bottom) having zero taper, positive taper and negative taper. The elliptical hole is drilled in 250 μm thick stainless steel (440) and is shown from a top-down viewpoint to reveal the ~5:1 aspect ratio (radii of 156 μm x 33.5 μm). The side-by-side circular through-holes are shown from side view after the sample was cross-sectioned to reveal cylindrical taper of the holes. These holes were also drilled in 250 μm thick stainless steel (440), and the taper angles, from left to right, are 0°, +6° and -6°. The white lines were added by the image rendering software to guide the eye.

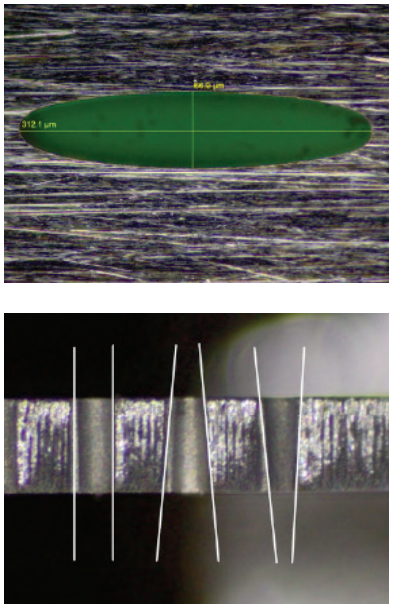

**Fig. 9:** Visible light microscope images of the top-down view of an elliptical through hole (top) and cross-sectional view of side-by-side circular through holes (bottom) with zero taper, positive taper and negative taper, from left to right, in stainless steel coupons.

Using the femtosecond laser trepanning process, a multitude of through-hole geometries can be created, beyond the simple ellipticity and taper control shown here. This new flexibility is widening the design space for fuel injector spray hole geometry. While the basic zero-taper, circular hole geometry readily achieved with this process is sufficient for current GDI fuel injector fabrication, the new geometrical flexibility may enable greater control of spray patterns and improved engine combustion. In the next section, we illustrate how the flexibility inherent with femtosecond laser processing extends beyond drilled hole geometries in metals to address laser machining of polymers—among other difficult-to-machine materials—as well as non-machining applications such as laser marking.

## 6. Materials Flexibility

In this final section, we demonstrate precision machining of polycarbonate, for a microfluidics application, along with gray-scale coloration of a polished stainless steel surface. At present, these are not high production volume applications for femtosecond laser processing. However, they could become high production volume applications in the near future and, moreover, represent the diverse array of unique femtosecond laser application capabilities.

Soft dielectrics, e.g. polymers, are traditionally very difficult to machine by mechanical or laser methods. Mechanical tools can deform the polymer substrate as it is machined. Conventional lasers can melt and chemically change the polymer material, causing change to the intrinsic viscosity (IV) and incompatibility with the end-application requirements. In contrast, femtosecond ablation can achieve precise machining with no appreciable change to the remaining polymer material.

As example, Fig. 10 shows a visible light photograph of a NASA check valve—a microfluidic system flow control component—machined from a solid sheet of 275 μm thick polycarbonate [30]. The central circular feature is the valve cap (1516 μm diameter), and the curved struts (234 μm strut width) provide flexible suspension of the cap. The fluid flow direction is normal to the image plane. The machining process used a Raydiance R-100 laser and a two-axis galvo scanner with f-theta lens for raster scanning the laser beam. Laser process parameters include: 45 μJ on target, 10 kHz pulse repetition rate, 30 μm focal spot diameter, and 1 minute total process time.

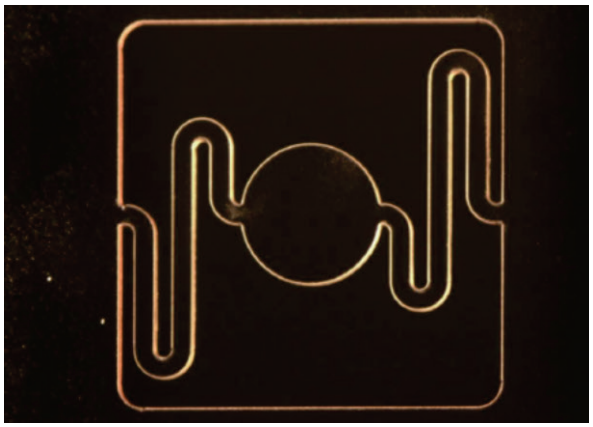

**Fig. 10:** NASA microfluidic check valve machined from 275 μm thick polycarbonate using a Raydiance laser workstation.

Conventional laser marking produces visible contrast marks by machining surface reliefs and/ or by scorching the material to yield discoloration by chemical change. In contrast, femtosecond laser marking can produce surface texturing with highly controllable degrees of light and dark

contrast that depend only upon the number of pulses delivered to each spot on the material surface. Fig. 11 shows an example of gray-scale coloration of a polished stainless steel surface. Each square of the checkerboard pattern has received a different number of pulses, and the squares exhibit very different surface textures and macroscopic marking contrast. The inset images show higher magnification of the surface morphology for the lightest (top, right) and darkest (bottom, right) squares. In creation of these textures, there was no detectable material removal and no observable HAZ to the substrate.

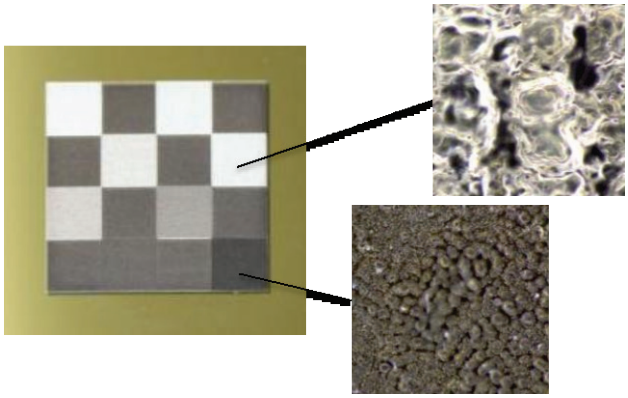

**Fig. 11:** A grid (left) of gray-scale colorations by surface texturing with a Raydiance laser on the surface of polished stainless steel. The insets (right) reveal different surface morphologies for light (top) vs. dark (bottom) zones of the grid.

Femtosecond laser machining of polymers, surface texturing metals for purpose of coloration, and many, many other applications of femtosecond lasers for materials processing have been shown in the academic literature [31][32] over the past several decades. We show these examples in this section not as demonstrations of novel effects. Rather, we display these examples as evidence that our commercial grade femtosecond laser systems can achieve all the high-value processing effects relevant to commercial markets. These are the benefits of using pulsed laser light in the sub-picosecond regime and the commercial grade form factor of fiber optics and autonomous laser control for reliable precision microfabrication tools.

## 7. Summary

Precision manufacturing industries are now leveraging femtosecond laser technology owing to the recent development of our true commercial grade femtosecond laser platform based on a fiber-optic photonics layer and autonomous, embedded software control system. The need for stable, reliable femtosecond laser systems for realistic manufacturing environments is clearly evident based on pulse width dependency for process quality, speed, and repeatability. With femtosecond laser microfabrication tools now accessible to industry, the relevance of femtosecond lasers to modern manufacturing has become clear based on compelling economics, unparalleled precision, and new flexibility with respect to materials. These new capabilities are opening up enormous opportunities in automotive components, consumer electronics, medical devices, aerospace and bioscience applications. Femtosecond laser materials processing simply provides faster, better and cheaper ways of fabricating precision parts in a wide array of high value applications.

## References


[1] Banks, P.S., Stuart, B.C., Komashko, A.M., Feit, M.D., Rubenchik, A.M., & Perry, M.D. "Femtosecond Laser Materials Processing," Proc. SPIE 3934, p.14 (2000).

[2] Chichkov, B.N., Momma, C., Nolte, S., von Alvensleben, F., and Tünnermann, A., "Femtosecond, picosecond and nanosecond laser ablation of solids," Appl. Phys. A 63, pp.109 (1996).

[3] Wellershoff, S.S., Hohlfeld, J., Güdde, J., & Matthias, E. "The role of electron-phonon coupling in femtosecond laser damage of metals," Appl. Phys. A 69 [Suppl.], S99 (1999).

[4] Korte, F., Nolte, S., Chichkov, B.N., Bauer, T., Kamlage, G., Wagner, T., Fallnich, C., & Welling, H. "Far-field and near-field material processing with femtosecond laser pulses," Appl. Phys. A 69 [Suppl.], S7 (1999).

[5] Zhu, X., "A new method for determining critical pulse width in laser material processing," Applied Surface Science 167, pp.230 (2000).

[6] Mielke, M. & Gaudiosi, D. "Nitinol machining rate dependence on pulse duration in the ultrafast laser regime," OSA CLEO/QELS Paper # JTuC3 (2010).

[7] Walter, D., Michalowski, A., & Dausinger, F., "Real-time monitoring and control of laser micro drilling using optical process emissions," Proc. Fourth International WLT-Conference on Lasers in Manufacturing, pp.569 (2007).

[8] Ancona, A., Jauregui, C., Doring, S., Roser, F., Limpert, J., Nolte, S., & Tunnermann, A., "Ultrashort pulse laser drilling of metals using a high repetition rate, high average power fiber CPA system," SPIE Proc. 7203 (2009).

[9] Mannion, P.T., Favre, S.F., Ivanov, D.S., O'Connor, G.M., Glynn, T.J., Lunney, J.G., & Doggett, B., "Langmuir Probe Investigation of Plasma Expansion in Femto- and Picosecond Laser Ablation of Selected Metals," J. Phys.: Conference Series, (COLA'05 proceedings).

[10] Shirk, M.D., & Molian, P.A., "A review of ultrashort pulsed laser ablation of materials," J. Laser Appl. 10, pp.18 (1998).

[11] Moulton, P.F., "Spectroscopic and laser characteristics of Ti:Al2O3", J. Opt. Soc. B 3, pp. 125 (1986).

[12] Zaouter, Y., Boullet, J., Mottay, E., & Cormier, E., "Generation of high energy and high quality ultrashort pulses in moderately non-linear fiber chirped pulse amplifier," SPIE 7195, 719512 (2009).

[13] Giesen, A., and Speiser, J., "Fifteen years of work on thin-disk lasers: results and scaling laws," IEEE JSTQE 13, pp. 598-609 (2007).

[14] Liu, Y., "A Strategic Study of Technological Innovations in the Fiber Optical Communications Industry," MBA thesis, Massachusetts Institute of Technology (2001).

[15] Digonnet, M.J.F., Rare-Earth-Doped Fiber Lasers and Amplifiers, 2nd edn., CRC Press, Boca Raton, FL (2001).
[16] Strickland, D., and Mourou, G., "Compression of amplified chirped optical pulses", Opt. Commun. 56, 219 (1985).
[17] Wielandy, S., Fishteyn, M., & Zhu, B. "Optical performance monitoring using nonlinear detection," J. Lightwave Technol. 22, pp.784 (2004).
[18] International Organization for Standardization (ISO), "Optics and photonics – Lasers and laser-related equipment – Test methods for laser beam power, energy and temporal characteristics," ISO 11554 (2006).
[19] Mielke, M., Gaudiosi, D., Hamamoto, M., Kim, K., Cline, R., and Sapers, S., "Pulse width stabilization for ultrafast laser systems," Physics Procedia 12, pp. 440-447 (2011).
[20] Mechanical shock and vibration testing was conducted by Pira International (Sunnyvale, CA) following ASTM Standards D3332 and D3580.
[21] Stifel Nicolaus, "Commercial laser and photonics industry," Equity Research Industry Analysis (Spring 2012).
[22] Strategies Unlimited, "The Worldwide Market for Lasers – Market Review and Forecast," pp. 99, 4th Ed. (2010).
[23] "Technologies for Achieving the Proposed Federal GHG and CAFÉ Standards 2017-2025 Light-Duty Vehicles," EPA & NHTSA presentation at the 2012 SAE Government and Industry Meeting.
[24] U.S. EPA, DOT & NHTSA, "Light-Duty Vehicle Greenhouse Gas Emission Standards and Corporate Average Fuel Economy Standards; Final Rule," (2010).
[25] Befrui, B., Corbinelli, G., Spiekermann, P., & Shost, M., "Large Eddy Simulation of GDI Single-Hole Flow and Near-Field Spray," SAE Int. J. Fuels Lubr. 5(2):2012.
[26] Kennedy, B. "Turbocharged holemaking," Micromanufacturing 3(4), pp.18-24 (2010).
[27] Cusanelli, G., "Microholes feasibility with regard to diesel and gasoline direct-injection needs," Engine Expo 2009, Stuttgart, Germany.
[28] Broers, A., Hoole, A., and Ryan, J., "Electron beam lithography—Resolution limits," Microelectronic Engineering 32, pp.131-142 (1996).
[29] Hung, D., Harrington, D., Gandhi, A., Markle, L., Parrish, S., Shakal, J., Sayar, H., Cummings, S., and Kramer, J., "Gasoline fuel injector spray measurement and characterization – a new SAE J2715 recommended practice," SAE Technical Paper Series 2008-01-1068 (2008).
[30] This work was conducted under a cooperative agreement funded by the Advanced Capabilities Division in NASA's Exploration Systems Mission Directorate (Ames Research Center). Contact: Rachel Prucey, 650-604-0643, rachel.l.prucey@nasa.gov
[31] Khan Malek, C., Robert, L., and Salut, R., "Femtosecond laser machining and lamination for large-area flexible organic microfluidic chips," Eur. Phys. J. Appl. Phys. 46, 12503 (2009).
[32] Vorobyev, A. and Guo, C., "Colorizing metals with femtosecond laser pulses," Appl. Phys. Lett. 92, 041914 (2008).

(Received: July 5, 2012, Accepted: July 14, 2013)